

Electron vortices generation of photoelectron of H_2^+ by counter-rotating circularly polarized attosecond pulses

Haojing Yang(杨浩婧), Xiaoyu Liu(刘晓煜), Fengzheng Zhu(朱风筝), Liguang Jiao(焦利光), and Aihua Liu(刘爱华)
Citation: Chin. Phys. B, 2024, 33 (**1**): 013303. DOI: 10.1088/1674-1056/ad011a
Journal homepage: http://cpb.iphy.ac.cn; http://iopscience.iop.org/cpb

What follows is a list of articles you may be interested in

Elliptically polarized high-order harmonic generation in nitrogen molecules with cross-linearly polarized two-color laser fields

Chunyang Zhai(翟春洋), Yinmeng Wu(吴银梦), Lingling Qin(秦玲玲), Xiang Li(李翔), Luke Shi(史璐珂), Ke Zhang(张可), Shuaijie Kang(康帅杰), Zhengfa Li(李整法), Yingbin Li(李盈傧), Qingbin Tang(汤清彬), and Benhai Yu(余本海)
Chin. Phys. B, 2023, 32 (**7**): 073301. DOI: 10.1088/1674-1056/acad70

Generation of quasi-chirp-free isolated attosecond pulses from atoms under the action of orthogonal two-color combined pulse of fundamental frequency and higher intensity second harmonic fields

Rui-Xian Yu(蔚瑞贤), Yue Qiao(乔月), Ping Li(李萍), Jun Wang(王俊), Ji-Gen Chen(陈基根), Wei Feng(冯伟), Fu-Ming Guo(郭福明), and Yu-Jun Yang(杨玉军)
Chin. Phys. B, 2023, 32 (**6**): 063302. DOI: 10.1088/1674-1056/acc80a

Attosecond spectroscopy for filming the ultrafast movies of atoms, molecules and solids

Lixin He(何立新), Xiaosong Zhu(祝晓松), Wei Cao(曹伟), Pengfei Lan(兰鹏飞), and Peixiang Lu(陆培祥)
Chin. Phys. B, 2022, 31 (**12**): 123301. DOI: 10.1088/1674-1056/aca6d2

Amplitude and rotation of the ellipticity of harmonicsfrom a linearly polarized laser field

Ping Li(李萍), Na Gao(高娜), Rui-Xian Yu(蔚瑞贤), Jun Wang(王俊), Su-Yu Li(李苏宇), Fu-Ming Guo(郭福明), and Yu-Jun Yang(杨玉军)
Chin. Phys. B, 2022, 31 (**10**): 103303. DOI: 10.1088/1674-1056/ac8ce8

Enhancement of isolated attosecond pulse generation by using long gas medium

Yueying Liang(梁玥瑛), Xinkui He(贺新奎), Kun Zhao(赵昆), Hao Teng(滕浩), and Zhiyi Wei(魏志义)
Chin. Phys. B, 2022, 31 (**4**): 043302. DOI: 10.1088/1674-1056/ac29a8

Electron vortices generation of photoelectron of H_2^+ by counter-rotating circularly polarized attosecond pulses

Haojing Yang(杨浩婧)[1], Xiaoyu Liu(刘晓煜)[1], Fengzheng Zhu(朱风筝)[2], Liguang Jiao(焦利光)[3,4,†], and Aihua Liu(刘爱华)[1,5,‡]

[1] *Institute of Atomic and Molecular Physics, Jilin University, Changchun* 130012, *China*
[2] *School of Mathematics and Physics, Hubei Polytechnic University, Huangshi* 435003, *China*
[3] *College of Physics, Jilin University, Changchun* 130012, *China*
[4] *Helmholtz-Institut Jena, D*-07743 *Jena, Germany*
[5] *State Key Laboratory of Transient Optics and Photonics, Chinese Academy of Sciences, Xi'an* 710119, *China*

(Received 31 August 2023; revised manuscript received 28 September 2023; accepted manuscript online 7 October 2023)

Molecular-frame photoelectron momentum distributions (MF-PMDs) of an H_2^+ molecule ion in the presence of a pair of counter-rotating circularly polarized attosecond extreme ultraviolet laser pulses is studied by numerically solving the two-dimensional time-dependent Schrödinger equation within the frozen-nuclei approximation. At small time delay, our simulations show that the electron vortex structure is sensitive to the time delay and relative phase between the counter-rotating pulses when they are partially overlapped. By adjusting time delay and relative phase, we have the ability to manipulate the MF-PMDs and the appearance of spiral arms. We further show that the internuclear distance can affect the spiral vortices due to its different transition cross sections in the parallel and perpendicular geometries. The lowest-order perturbation theory is employed to interpret these phenomena qualitatively. It is concluded that the internuclear distance-dependent transition cross sections and the confinement effect in diatomic molecules are responsible for the variation of vortex structures in the MF-PMDs.

Keywords: photoelectron momentum distribution, attosecond pulse, vortex

PACS: 33.80.–b, 42.65.Re, 87.15.mn, 87.15.ht **DOI:** 10.1088/1674-1056/ad011a

1. Introduction

The rapid development of ultrashort laser pulse technology[1–3] has provided essential tools for investigating electron dynamics in atoms, molecules, and solids, which bear the promise of electron control in matter. Many ultrafast measurement techniques, such as phasemeters,[4] streaking cameras,[5,6] and attoclocks,[7] are based upon photoionization and the subsequent induced processes. In recent years, elliptically or circularly polarized attosecond pulses and their combinations have been used to probe atomic and molecular structures using photoelectron momentum distributions (PMDs).[8–15] The PMD originating from the ionization of atoms and molecules by intense laser pulses convey valuable and fruitful information about the target electrons. Different parts of PMD not only reflect certain aspects of the target structure information but also encode different ionization dynamics in the laser-matter interaction. Both the atomic and molecular PMDs under extreme ultraviolet (XUV) laser have been investigated by many theoretical groups. For example, Murakami and Chu[16] exemplified the mechanism of symmetry breaking in the H atom PMD. Wu and He[11] showed that atomic PMD under two-color XUV lasers can be affected by both the relative phase and time delay between the two lasers. Yuan *et al.*[15,17] proved the dependence of molecular-frame photoelectron momentum distribution (MF-PMD) on molecular orbital symmetry. Furthermore, the interference between directly ionized electrons and rescattered electrons can also affect MF-PMD. The photoionization of H_2^+ molecular ion by elliptically polarized UV laser pulses has been studied by Zhang *et al.*,[8] and it has been shown that the MF-PMD depends further on the laser ellipticity and internuclear distance.

The experimental investigations on PMDs for understanding the structure information and ionization dynamics of atoms and molecules are also continuing.[18,19] Odenweller *et al.*[19] studied the electron emission from the H_2^+ molecule ion and found that the complex laser-driven electron dynamics can be encoded in the unexpected PMD.

In recent years, creating and manipulating vortex states of light beams[20,21] and electron vortices[10,21–25] have attracted considerable attention, since vortices can be characterized by intrinsic orbital angular momentum in, *e.g.*, twisted light beams and electron beams. Taking the hydrogen atom as an example, the vortex quasiparticles in the atomic wavefunctions were studied under the short rectangular half-period electric field pulse.[26] When two circularly polarized laser pulses are used for ionization of atoms or molecules, the vortex-shaped momentum distributions[24,27] has been discovered as a new feature of laser-induced electron wavepackets interfer-

†Corresponding author. E-mail: lgjiao@jlu.edu.cn
‡Corresponding author. E-mail: aihualiu@jlu.edu.cn

© 2024 Chinese Physical Society and IOP Publishing Ltd

ence. The time-delayed counter-rotating circularly polarized attosecond pulses were proposed to generate vortex-shaped photoelectron wave packets in the photoionization of helium atom[22,28] and hydrogen molecular ion.[29]

Electron vortex is generated in the counter-rotating circularly polarized laser field. The electron vortex structure[22] caused by the interference effect of two pulses has a time delay that changes within one cycle.[30] The vortices in molecular photoionization[26,28,31] was studied by applying either the photoionization of monochromatic field[24,25] or dichromatic field.[10,24,26,28] In addition to the time delay, the control of other laser parameters is also an interesting topic discussed by many researchers. It is shown that the photoelectron momentum, electron ejection angle, relative carrier envelope phase, and time delay between two circularly polarized pulses are related to spiral vortices. Furthermore, vortices are found not only in photoionization, but also photodetachment[31,32] and photodissociation.[29]

The simplest molecule H_2^+ has served as an ideal prototype to explore the ultrafast dynamics in diatomic molecules, such as high harmonic generation,[33–35] the double-slit interference effect,[36,37] the dissociation of molecule,[29,38,39] and so on.

In the present work, we investigate the interaction of H_2^+ molecule ion with a pair of counter-rotating circularly polarized laser pulses. The ultrafast attosecond timescale allows us to ignore the rotational and vibrational effects of atomic nuclei,[40–42] which are in picosecond and femtosecond timescales, respectively.

This paper is structured as follows. In Section 2 we briefly introduce the numerical method and model system for solving the time-dependent Schrödinger equation (TDSE) and extracting physical observable. The simulation results and corresponding discussion are presented in Section 3. The summary and conclusion are made in Section 4. Unless specifically stated otherwise, atomic units (a.u.) $\hbar = m_e = e = 1$ are used throughout this paper.

2. Theory and models

For an aligned homonuclear diatomic molecule in the presence of an ultrashort laser pulse, we can ignore the vibrational and rotational degrees of molecules and only consider electronic movement under the combination of electric field from external laser field and the electrostatic field from molecular nuclei.[37,40] In the circularly polarized laser fields, a reduced two-dimensional (2D) model can be employed to capture the essential physical significance. In this work, we adopt the reduced 2D TDSE under the frozen-nuclei approximation as follow:

$$\mathrm{i}\frac{\partial \psi(x,y,t)}{\partial t} = H\psi(x,y,t), \tag{1}$$

where the system Hamiltonian $H = T + V_0(x,y) + \boldsymbol{r}\cdot\boldsymbol{E}(t)$ includes the kinetic energy term of electron $T = (p_x^2 + p_y^2)/2$ and the field-free potential $V_0(x,y)$,

$$V_0(x,y) = -\frac{1}{\sqrt{(x-R_c/2)^2 + y^2 + a}} - \frac{1}{\sqrt{(x+R_c/2)^2 + y^2 + a}}, \tag{2}$$

where $R_c = 2$ is the internuclear distance of H_2^+ molecular ion at equilibrium, and $a = 0.5$ is the soft-core parameter. For $R_c = 4$, we further employ the soft-core parameter $a = 0.73$ to correctly reproduce the ground state energy of H_2^+ molecular ion.

The interaction between external laser field and the electron is given by $V_I = \boldsymbol{r}\cdot\boldsymbol{E}(t)$. The laser electric field is described by

$$\boldsymbol{E}(t) = \boldsymbol{E}_1(t) + \boldsymbol{E}_2(t), \tag{3}$$

where $\boldsymbol{E}_1(t)$ and $\boldsymbol{E}_2(t)$ are two circularly polarized laser pulses in sequence with a time delay t_d

$$\boldsymbol{E}_1(t) = \frac{1}{\sqrt{2}}E_0 f(t)\left[\hat{e}_x\cos(\omega t + \phi_1) + \hat{e}_y\sin(\omega t + \phi_1)\right], \tag{4}$$

$$\boldsymbol{E}_2(t) = \frac{1}{\sqrt{2}}E_0 f(t-t_d)\left\{\hat{e}_x\cos\left[\omega(t-t_d) + \phi_2\right] \pm \hat{e}_y\sin\left[\omega(t-t_d) + \phi_2\right]\right\}, \tag{5}$$

where ϕ_1 and ϕ_2 are the carrier envelope phases (CEPs) and the sign $\pm$ denotes the helicity of (counter-clockwise or clockwise) circularly polarized laser pulses. A slowly varying temporal envelope function of $f(t) = \sin^2(\pi t/T)$ with duration $T = nT_0$ is employed here, where $T_0 = 2\pi/\omega$ is the optical cycle (o.c.). In this work, the pulse lasts for 10 optical cycles ($n = 10$). In our calculation, we focus on the single-photon ionization process, which means that the electron can be ionized by absorbing only one photon. In the present work, we choose the two laser fields with the wavelength of 30 nm ($\omega = 1.52 > I_p = 1.1$, where I_p is ionization energy of the ground state of H_2^+ molecular ion at $R_c = 2$) and the peak intensity of $I_0 = 10^{14}$ W/cm^2. The molecular alignment is set along the x axis.

This study utilizes the split-operator fast-Fourier transform algorithm to solve the 2D TDSE.[43] The real time propagation of wave function from t to $t + \Delta t$ can be expressed as

$$\psi(t+\Delta t) \approx \mathrm{e}^{-\mathrm{i}V\Delta t/2}\,\mathrm{e}^{-\mathrm{i}T\Delta t}\,\mathrm{e}^{-\mathrm{i}V\Delta t/2}\psi(t). \tag{6}$$

The initial state is set as the ground state of H_2^+ molecular ion, which can be obtained by imaginary time propagation with an arbitrary non-trivial state.

In our simulation, the spatial dimension ranges from -150 to 150, which contains 1024 grid points in both the x and y dimensions. A $\cos^{1/8}$ boundary absorber placed at $x, y = \pm 130$ is used to avoid the nonphysical reflection of wave functions. The step size of time propagation is set to be $\Delta t = 0.01$.

After the laser field is finished, wave functions are further propagated for an additional five optical cycles to ensure that all the ionized components of electron wave function are far away from the nuclei. Then we seperate the photoelectron wavepacket by applying the mask function. The ionized wave packet is obtained by $\psi_{\rm ion}(x,y) = [1-M(r_{\rm b})]\psi_{\rm final}(x,y)$. Here, $\psi_{\rm final}(x,y)$ is the wave packet at final time and $M(r_{\rm b})$ is a mask function

$$M(r_{\rm b}) = \begin{cases} 1, & r \le r_{\rm b}, \\ \exp[-\alpha(r-r_{\rm b})], & r > r_{\rm b}, \end{cases} \tag{7}$$

with $\alpha = 1$, $r = \sqrt{x^2+y^2}$, and $r_{\rm b} = 10$ which corresponds to the boundary of the bound-electron wave function. Finally, wave functions in momentum space can be obtained by applying Fourier transform to the ionized wave function as

$$\widetilde{\psi}(p_x,p_y) = \frac{1}{2\pi}\iint \psi_{\rm ion}(x,y)\,{\rm e}^{-{\rm i}(xp_x+yp_y)}\,{\rm d}x\,{\rm d}y. \tag{8}$$

The 2D MF-PMD is given by

$$\frac{\partial P}{\partial p_x \partial p_y} = |\widetilde{\psi}(p_x,p_y)|^2. \tag{9}$$

3. Results and discussion

In this work, the initial state of the hydrogen molecular ion H_2^+ is the ground state, which is denoted as $1s\sigma_g$. As the internuclear distance varies, the initial electron density distribution of the H_2^+ molecular ion also changes. This is illustrated in Figs. 1(a) and 1(b) for internuclear distances of $R_c = 2$ and 4, respectively. The wave function of the H_2^+ molecular ion can be approximately described as the symmetric superposition of the wave functions of two hydrogen atoms positioned along the molecular axis at $\pm R_c/2$. In the case of equilibrium at $R_c = 2$, the electron densities of the two hydrogen atoms overlap significantly, resulting in an ionization potential energy of $I_p = 1.1$. However, when $R_c = 4$, the overlapping between the two hydrogen atoms is reduced, leading to a decrease in the ionization potential energy to $I_p = 0.79$.

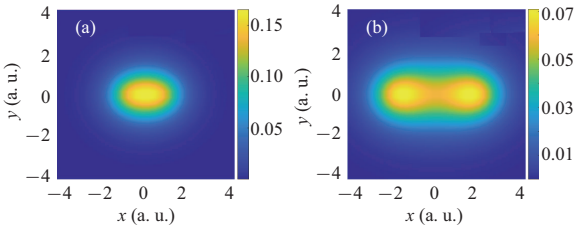


Fig. 1. The initial electron density distributions of H_2^+ in the ground state ($1s\sigma_g$) at two different internuclear distances: (a) $R_c = 2$, (b) $R_c = 4$.

We first investigate the MF-PMDs of H_2^+ molecule ions under the influence of a pair of counter-rotating circularly polarized attosecond pulses at various time delays t_d. In the left panels of Fig. 2, we demonstrate the MF-PMDs of the H_2^+ molecule ion by left and right circularly polarized laser pulses with time delays of 0, 1, and 1.5 o.c., respectively. The right panels depict the corresponding Lissajous figures of the electric fields. The comparison among these three situations indicates that different time delay results in very different distribution patterns in the MF-PMDs. In the top two panels, when there is no time delay between two counter-rotating pulses, the total electric field is reduced to a purely linearly polarized pulse along the x axis, and parallel to the molecular alignment axis. In this case, the MF-PMD is a typical six-petal structure.[41,44] The two panels in the middle row display the MF-PMD (left) and corresponding Lissajous curve (right) in the case of 1 o.c. time delay between two counter-rotating pulses in sequence. From Fig. 2(b), it can be seen that when $t_d = 1$ o.c., the electric field mainly lies along the x axis. The corresponding MF-PMD show a significant vortex structure. When the time delay is continuously increased to $t_d = 1.5$ o.c., the total field has both x and y components, with peak intensity in y axis stronger than that in x axis. The MF-PMD demonstrates dominant distribution in the p_y direction, which is similar to the MF-PMD of H_2^+ in the perpendicular geometry, as discussed in Ref. [44].

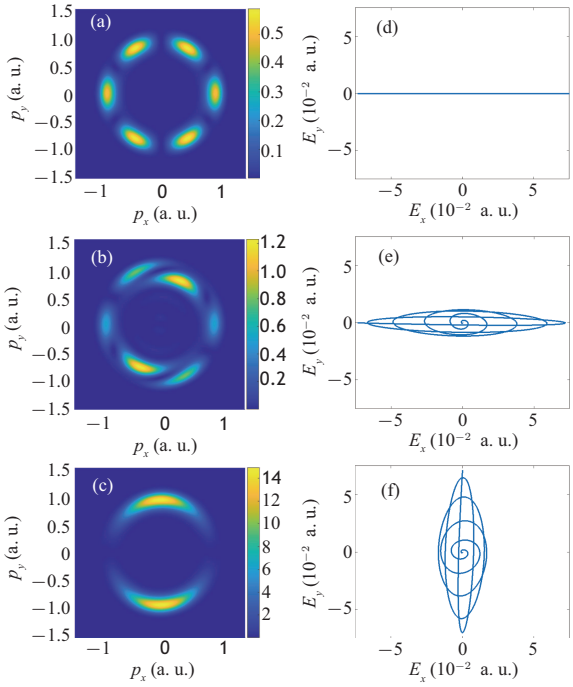


Fig. 2. The MF-PMDs (left panels) and corresponding Lissajous curves of electric field (right panels). The H_2^+ sits at its equilibrium internuclear distance $R_c = 2$. From top to bottom panels, the time delay are 0, 1, and 1.5 o.c., respectively. The laser parameters are: central carrier frequency $\omega = 1.52$, peak intensity $I_0 = 10^{14}$ W/cm^2, the carrier envelope phase $\phi_1 = \phi_2 = 0$, and pulse duration $\tau = 1.0$ fs.

Our numerical results can be understood by the attosecond perturbation ionization theory.[45,46] For H_2^+ molecule ions with two identical centers, the corresponding MF-PMD can be approximated by the superposition of the ionization probabilities of two identical hydrogen atoms. For circularly polarized pulses, the photo-ionization in the x and y directions

can be obtained by calculating the modular squares of the transition amplitude in the x and y directions,[15]

$$|A_{\sigma_g}^{(x)}|^2 \propto 2|\sigma^{(x)}|^2 E_x^2 \cos^2\theta \cos^2\left(\frac{\boldsymbol{p}\cdot\boldsymbol{R}}{2}\right)\psi_{1s}^2(|p|), \quad (10)$$

$$|A_{\sigma_g}^{(y)}|^2 \propto 2|\sigma^{(y)}|^2 E_y^2 \cos^2\theta \cos^2\left(\frac{\boldsymbol{p}\cdot\boldsymbol{R}}{2}\right)\psi_{1s}^2(|p|), \quad (11)$$

where $\sigma^{(x)}$ and $\sigma^{(y)}$ are x- and y-geometry transition cross sections, and θ is the angle between the electron momentum p and molecular axis (that is x axis). The total photoelectron momentum distribution P can be decomposed into two components

$$P = |A_{\sigma_g}|^2 = |A_{\sigma_g}^{(x)}|^2 + |A_{\sigma_g}^{(y)}|^2 = P_x + P_y, \quad (12)$$

where P_x and P_y are the ionization probabilities due to the x and y components of the electric field, respectively. The photoelectron momentum distribution is linearly related to the electric field amplitude and transition cross section.

The cross section $\sigma^{(x)}$ related to the parallel geometry transition to σ_u ($m = 0$), and $\sigma^{(y)}$ is connected to the vertical transition π_u ($m = \pm 1$), therefore they can also be rewritten as $\sigma_\parallel$ and $\sigma_\perp$, respectively. At $R_c = 2$, the transition cross sections from the ground state to σ_u and π_u are $\sigma_\perp = 528.5$ kb and $\sigma_\parallel = 38.95$ kb, respectively.[41] The contribution of the π_u (vertical transition geometry) channel is more significant than that of the σ_u (parallel transition geometry) channel. The significant difference between parallel and perpendicular geometries are demonstrated obviously in Figs. 2(a) and 2(c). In panel (a), the y component of the electric field is canceled due to the 0 time delay between two counter-rotating pulses, therefore the MF-PMD is characterized by the typical structure in the parallel geometry.[40] In Fig. 2(c), although the electric field in x axis does not vanish, its magnitude is much smaller than that in y axis. Considering that $\sigma_\perp \gg \sigma_\parallel$, the contribution of parallel geometry is negligible, and perpendicular geometry is dominant, no obvious vortex structure can be observed.

However, we can adapt the relative ratio between the parallel and perpendicular geometries, which makes them comparable. In Fig. 2(b), when the time delay is 1 o.c., the total combined electric field has much smaller y component than the x component. Considering the fact that $\sigma_\perp \gg \sigma_\parallel$, the ionization yield in parallel and perpendicular geometries are expected to be comparable, strong interference effect and electron vortex structure can be observed. Although this is single photon single ionization, we should expect two spiral arms only, but there are "six spiral arms". Such "six-spiral-arm" structure is due to the contribution of parallel geometry which has six-petal structure from the confinement effect.[41] The difference phase in parallel and perpendicular geometries produces strong interference between them, which gives birth to the vortex structure.

In the scenario of atomic spirals,[22,24,30,47], the interference between $\pm m$ ($m \neq 0$) partial waves plays a crucial role in the formation of vortex structures. To understand the vortex structure of H_2^+, it is essential to examine the m value of the photoelectron in the final state. Clearly, in case of Figs. 2(a) and 2(d), only the $m = 0$ partial wave contributes to the final state of the electron. On the other hand, for the other cases, both $m = 0$ and $m = \pm 1$ partial waves can be present in the final state. The interference of all three partial waves will eventually results in more intricate vortex structures than the two-spiral-arm vortex, assuming that the yield of each partial wave is comparable.

From the above discussion, we know that the vortex structure appears if the yields of parallel and perpendicular geometries are comparable. To achieve such a condition, we can manipulate the relative phase and time delay simultaneously. If the time delay is small enough to ensure a large overlapping between two pulses, we can always adjust the laser parameters to keep $E_x^{\max} \approx 4E_y^{\max}$.

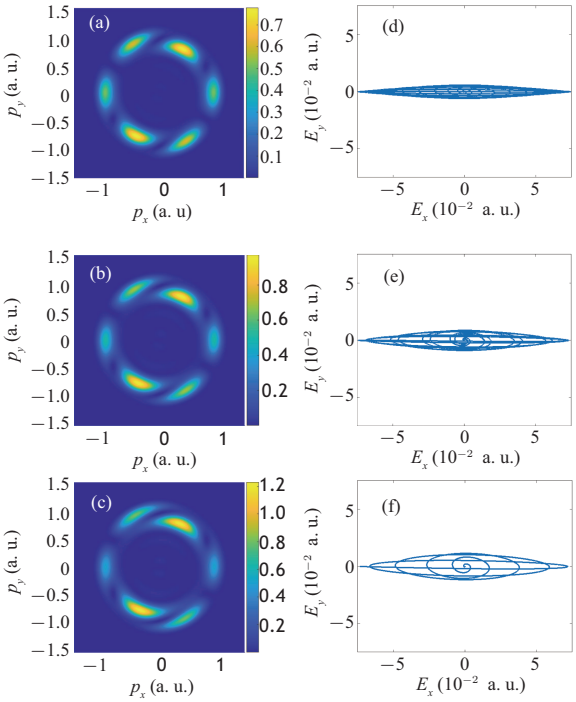


Fig. 3. The MF-PMDs (left panels) and corresponding Lissajous curves of electric field (right panels). From top to bottom panels: (a) and (d) $t_d = 0.5$ o.c., $\phi_1 = \pi$, $\phi_2 = 0$; (b) and (e) $t_d = 0.75$ o.c., $\phi_1 = 0.5\pi$, $\phi_2 = 0$; (c) and (f) $t_d = 1$ o.c., $\phi_1 = \phi_2 = 0$. The rest laser parameters are: central carrier frequency $\omega = 1.52$, peak intensity $I_0 = 10^{14}$ W/cm^2, and pulse duration $\tau = 1.0$ fs. The H_2^+ sits at its equilibrium internuclear distance $R_c = 2$.

In Fig. 3, we demonstrate several examples that produce visible "six-spiral-arm" vortex structure. In the top panels, $t_d = 0.5$ o.c., $\phi_1 = \pi$, $\phi_2 = 0$; in the middle panels, $t_d = 0.75$ o.c., $\phi_1 = 0.5\pi$, $\phi_2 = 0$; and the bottom panels have $t_d = 1$ o.c., $\phi_1 = \phi_2 = 0$. In top panels, when the time delay is 0.5 o.c., the relative phase is $\phi_2 - \phi_1 = -\pi$. When the time delay is increased to 0.75 o.c., the relative phase should be adjusted as $\phi_2 - \phi_1 = -\pi/2$. Then in the bottom panels,

if the time delay is 1 o.c., the relative phase difference need to be set as $\phi_2 - \phi_1 = 0$. All graphs in left panels give very similar "six-spiral-arm" vortex structure. To maintain the similar MF-PMDs, 2π relative phase compensation is required for per optical cycle time delay increasing. As the time delay expands, the spiral arms in MF-PMDs become more elongated and slender.[48] In addition, as the time delay increases, the yield of the y-component laser field will continue to grow, and the yield of perpendicular geometry will become more pronounced.

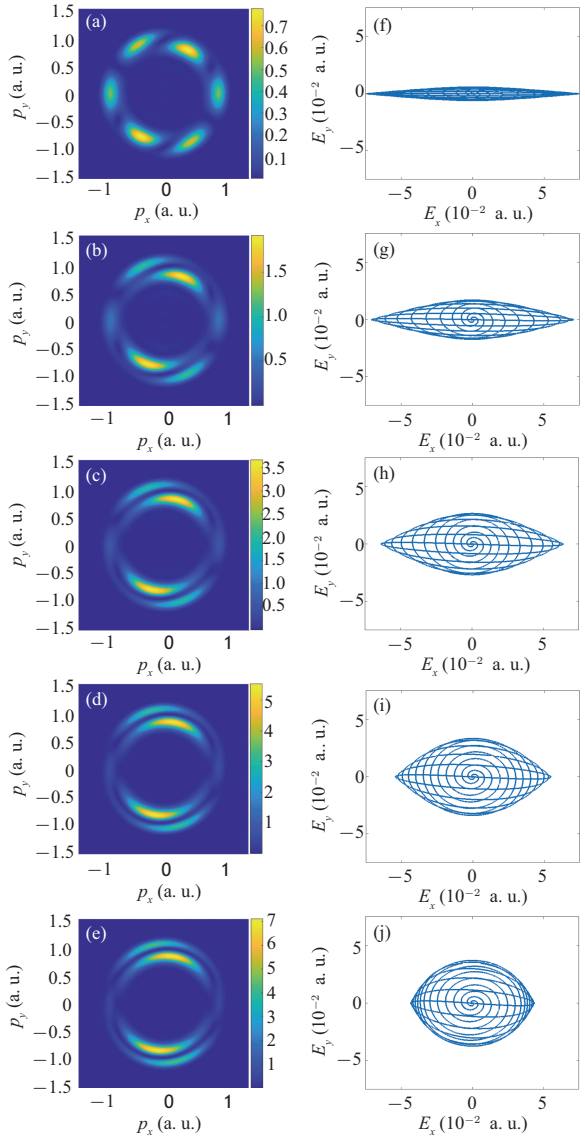


Fig. 4. The MF-PMDs (left panels) and corresponding Lissajous curves of electric field (right panels). The H_2^+ sits at its equilibrium internuclear distance $R_c = 2$. From top to bottom panels, the time delay are 0.5, 1.5, 2.5, 3.5, and 4.5 o.c., respectively. The rest laser parameters are: central carrier frequency $\omega = 1.52$, peak intensity $I_0 = 10^{14}$ W/cm^2, the carrier envelope phase $\phi_1 = \pi$, $\phi_2 = 0$, and pulse duration $\tau = 1.0$ fs.

Figure 4 demonstrates MF-PMDs for fixed phase difference at $\phi_2 - \phi_1 = \pi$, but vary the time delay from 0.5 o.c. to 4.5 o.c. by 1-o.c. increment. On the top two rows, where the time delay $t_d < 2$ o.c., the "six-spiral-arm" vortex structure are clearly visible. In the middle panels, when $t_d = 2.5$ o.c., the vortex structure still exists, but the two arms on the x axis diminish, and connect to the other arms. Since now $E_x^{max} \approx 2E_y^{max}$, it does not guarantee the comparable yields in both parallel and perpendicular geometries. If we further enlarge the time delay, as displayed in bottom two rows, $E_x^{max} \ll 4E_y^{max}$, the yield in parallel geometry is smeared out, and the MF-PMD reduces to "two-spiral-arm" vortex, which is typical vortex of single photon single ionization by a pair of counter-rotating circularly polarized attosecond pulses.[24]

Other than the equilibrium internuclear distance, the hydrogen molecular ion H_2^+ can vary its internuclear distance. As mentioned above, *e.g.*, H_2^+ with $R_c = 4$ has a different ground state energies. Actually, it also has different transition cross sections. Some early studies[41] showed that when $R_c = 4$, $\sigma_\parallel = 413.9$ kb, $\sigma_\perp = 284.8$ kb, the transition cross section in the x direction is slightly larger than that in the y direction. Therefore, we can expect different behavior when H_2^+ is radiated by the same counter-rotating circularly polarized pulses. In Fig. 5, we display the MF-PMDs (left panels) and the Lissajous curves of electric field (right panels) for H_2^+ with $R_c = 4$. All the laser parameters are the same as Fig. 2. In the top two rows, where $E_x^{max} \gg E_y^{max}$ and $\sigma_\parallel > \sigma_\perp$, the yield from parallel geometry dominates the MF-PMDs in both cases, because the yield of perpendicular geometry transition vanishes. Only in the case of bottom panels, when time delay $t_d = 1.5$ o.c., $E_y^{max} \approx 2E_x^{max}$, the yield from perpendicular geometry can be compared to that from parallel geometry transition, a clear "six-spiral-arm" vortex structure occurs. If we ignore the nodes that caused the confinement effect,[41,49] this vortex shows typical "two-spiral-arm" vortex in MF-PMD.

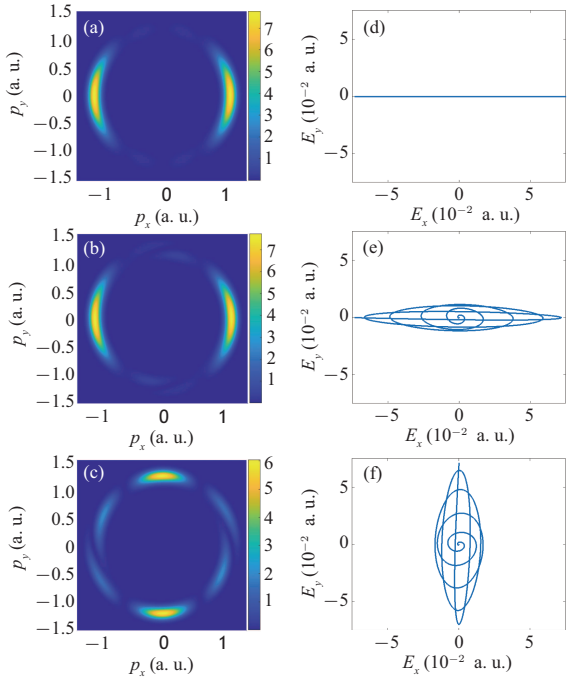


Fig. 5. The same as Fig. 2 but with different internuclear distance $R_c = 4$.

4. Summary and conclusions

In summary, by numerically solving the two-dimensional TDSE in the frozen-nuclei approximation, we have investigated the MF-PMDs of H_2^+ molecule ion by a pair of counter-rotating circularly polarized laser pulses with time delay. When the time delay is small enough that one component of the electric laser field is partially canceled, the regular "two-spiral-arm" vortex in single photon single ionization turns into "six-spiral-arm" vortex or smear out the vortex structure. These effects are due to the combination effect of different transition cross sections in parallel and perpendicular geometries, and the confinement effect of diatomic molecules. By simultaneously varying the phase and time delay of laser pulses, we can control the appearance and disappearance of such "six-spiral-arm".

For H_2^+ at non-equilibrium internuclear distance, the same behavior can be observed. However, due to the variation in transition cross sections and their relative ratio over R_c, the vortex generation parameters are different. For instance, the cases of $R_c = 2$ and 4 have opposite MF-PMDs when they have the same 0 relative phase and same $t_d = 1$ o.c. or 1.5 o.c. time delay. It implies the possibility of using molecular electron vortex as strong spectroscopic instruments to investigate molecular structure and dynamics. The clear distinction in MF-PMDs provides us a novel tool to identify the molecular structure information, *e.g.*, the chemical bond length. Additionally, the molecular vortex structure produced by counter-rotating circularly polarized pulses may be used to probe the electron dynamics in chiral molecules by photoelectron circular dichroism.[50]

In this work, we have only investigated the simplest molecular prototype system. Future research may be extended to more complex molecule, such as carbon dioxide, carbonyl sulfide or benzene which have many electrons.

Acknowledgements

Project supported by the Natural Science Foundation of Jilin Province, China (Grant No. 20220101016JC), the National Key Research and Development Program of China (Grant No. 2022YFE0134200), the National Natural Science Foundation of China (Grant Nos. 12174147, 91850114, and 11774131), the Open Research Fund of State Key Laboratory of Transient Optics and Photonics. Part of the numerical simulation was done on the high-performance computing cluster Tiger@IAMP in Jilin University.

References

[1] Brabec T and Krausz F 2000 *Rev. Mod. Phys.* **72** 545
[2] Krausz F and Ivanov M 2009 *Rev. Mod. Phys.* **81** 163
[3] Chang Z and Corkum P 2010 *J. Opt. Soc. Am. B* **27** B9
[4] Wittmann T, Horvath B, Helml W, Schätzel M G, Gu X, Cavalieri A L, Paulus G and Kienberger R 2009 *Nat. Phys.* **5** 357
[5] tatani J, Quéré F, Yudin G L, Ivanov M Y, Krausz F and Corkum P B 2002 *Phys. Rev. Lett.* **88** 173903
[6] Kitzler M, Milosevic N, Scrinzi A, Krausz F and Brabec T 2002 *Phys. Rev. Lett.* **88** 173904
[7] Eckle P, Smolarski M, Schlup P, Biegert J, Staudte A, Schöffler M, Muller H G, Dörner R and Keller U 2008 *Nat. Phys.* **4** 565
[8] Zhang H D, Ben S, Xu T T, Song K L, Tian Y R, Xu Q Y, Zhang S Q, Guo J and Liu X S 2018 *Phys. Rev. A* **98** 013422
[9] Yuan K J, Chelkowski S and Bandrauk A D 2015 *J. Chem. Phys.* **142** 144304
[10] Yuan K J, Chelkowski S and Bandrauk A D 2016 *Phys. Rev. A* **93** 053425
[11] Wu W Y and He F 2016 *Phys. Rev. A* **93** 023415
[12] Yuan K J and Bandrauk A D 2017 *Phys. Chem. Chem. Phys.* **19** 25846
[13] Yuan K J, Shu C C, Dong D and Bandrauk A D 2017 *J. Phys. Chem. Lett.* **8** 2229
[14] Yuan K J and Bandrauk A D 2019 *J. Phys. Chem. A* **123** 1328
[15] Yuan K J, Chelkowski S and Bandrauk A D 2015 *Chem. Phys. Lett.* **638** 173
[16] Murakami M and Chu S I 2016 *Phys. Rev. A* **93** 023425
[17] Yuan K J, Lu H and Bandrauk A D 2017 *Structural Chemistry* **28** 1297
[18] Xie X, Wang T, Yu S, Lai X, *et al*. 2017 *Phys. Rev. Lett.* **119** 243201
[19] Odenweller M, Takemoto N, Vredenborg A, Cole K, Pahl K, Titze J, Schmidt L P H, Jahnke T, Dörner R and Becker A 2011 *Phys. Rev. Lett.* **107** 143004
[20] Hernández-García C, Vieira J, Mendonca J T, Rego L, San Román J, Plaja L, Ribic P R, Gauthier D and Picón A 2017 *Photonics* **4** 28
[21] Shen Y, Wang X, Xie Z, Min C, Fu X, Liu Q, Gong M and Yuan X 2019 *Light: Science & Applications* **90** 697
[22] Djiokap J N, Meremianin A V, Manakov N, Hu S, Madsen L and Starace A F 2016 *Phys. Rev. A* **94** 013408
[23] Lloyd S, Babiker M, Thirunavukkarasu G and Yuan J 2017 *Rev. Mod. Phys.* **89** 035004
[24] Djiokap J N, Hu S, Madsen L, Manakov N, Meremianin A and Starace A F 2015 *Phys. Rev. Lett.* **115** 113004
[25] Li M, Zhang G, Kong X, Wang T, Ding X and Yao J 2018 *Opt. Express* **26** 878
[26] Ovchinnikov S Y, Sternberg J, Macek J, Lee T G and Schultz D R 2010 *Phys. Rev. Lett.* **105** 203005
[27] Harris M, Hill C and Vaughan J 1994 *Opt. Commun.* **106** 161
[28] Djiokap J N, Meremianin A, Manakov N, Hu S, Madsen L and Starace A F 2017 *Phys. Rev. A* **96** 013405
[29] Chen Z, He P L and He F 2020 *Phys. Rev. A* **101** 033406
[30] Zhen Q, Zhang H D, Zhang S Q, Ji L, Han T and Liu X S 2020 *Chem. Phys. Lett.* **738** 136885
[31] Vélez F C, Geng L, Kamiński J, Peng L Y and Krajewska K 2020 *Phys. Rev. A* **102** 043102
[32] Geng L, Vélez F C, Kamiński J, Peng L Y and Krajewska K 2020 *Phys. Rev. A* **102** 043117
[33] Guo Y, Liu A, Wang J and Liu X 2019 *Chin. Phys. B* **28** 094212
[34] Han J X, Wang J, Qiao Y, Liu A H, Guo F M and Yang Y J 2019 *Opt. Express* **27** 8768
[35] Wang J, Liu A and Yuan K J 2020 *Opt. Commun.* **460** 125216
[36] Horner D A, Miyabe S, Rescigno T N, McCurdy C W, Morales F and Martín F 2008 *Phys. Rev. Lett.* **101** 183002
[37] Guan X, Secor E B, Bartschat K and Schneider B I 2012 *Phys. Rev. A* **85** 043419
[38] Gräfe S, Engel V and Ivanov M Y 2008 *Phys. Rev. Lett.* **101** 103001
[39] He F, Becker A and Thumm U 2008 *Phys. Rev. Lett.* **101** 213002
[40] Guan X, Secor E B, Bartschat K and Schneider B I 2011 *Phys. Rev. A* **84** 033420
[41] Guan X, DuToit R C and Bartschat K 2013 *Phys. Rev. A* **87** 053410
[42] Yuan K J and Bandrauk A D 2012 *Phys. Rev. A* **85** 013413
[43] Feit M, Fleck J Jr and Steiger A 1982 *J. Comput. Phys.* **47** 412
[44] Liu X Y, Gao S, Liu A, Jiao L G and Zhu F Z 2023 *Commun. Theor. Phys.* **75** 035503
[45] Pronin E A, Starace A F, Frolov M V and Manakov N L 2009 *Phys. Rev. A* **80** 063403
[46] Pronin E A, Starace A F and Peng L Y 2011 *Phys. Rev. A* **84** 013417
[47] Yuan K J and Bandrauk A D 2015 *Phys. Rev. A* **92** 063401
[48] Ma M Y, Wang J P, Jing W Q, Guan Z, Jiao Z H, Wang G L, Chen J H and Zhao S F 2021 *Opt. Express* **29** 33245
[49] Fernández J, Fojón O, Palacios A and Martín F 2007 *Phys. Rev. Lett.* **98** 043005
[50] Pengel D, Kerbstadt S, Englert L, Bayer T and Wollenhaupt M 2017 *Phys. Rev. A* **96** 043426